JOURNAL OF THERMOPHYSICS AND HEAT TRANSFER
Vol. 20, No. 1, January–March 2006

Effect of Coriolis and Centrifugal Forces at High Rotation and Density Ratios

Ahmad Sleiti* and J. S. Kapat†
University of Central Florida, Orlando, Florida 32816-2450

Numerical simulation of fluid flow and heat transfer of high rotation and density ratio flow in internal cooling channels of turbine blades with smooth walls is the main focus of this study. The flow in these channels is affected by rotation, buoyancy, bends, and boundary conditions. On the basis of comparison between two-equation ($k-\varepsilon$ and $k-\omega$) and Reynolds-stress (RSM) turbulence models, it is concluded that the two-equation turbulence models cannot predict heat transfer correctly, whereas RSM showed improved prediction. Thus RSM model was validated against available experimental data (which are primarily at low rotation and buoyancy numbers). The model was then used for cases with high rotation numbers (as much as 1.29) and high-density ratios (up to 0.4) not studied previously. Particular attention was given to how Reynolds stresses, turbulence intensity, and transport are affected by coriolis and buoyancy/centrifugal forces caused by high levels of rotation and density ratio. The results obtained are explained in view of physical interpretation of Coriolis and centrifugal forces. It has been concluded that the heat-transfer rate can be enhanced rapidly by increasing rotation number to values that are comparable to the enhancement caused by introduction of ribs inside internal cooling channels. It is possible to derive linear correlation for the increase in Nusselt number as a function of rotation number. Increasing density ratios at high rotation number does not necessarily cause an increase in Nusselt number. The increasing thermal boundary-layer thickness near walls is the possible reason for this behavior of Nusselt number.

Nomenclature

a_{ce}	=	acceleration caused by centrifugal force
a_{co}	=	acceleration caused by Coriolis force
D_h	=	hydraulic diameter
f_{ce}	=	centrifugal force
f_{co}	=	Coriolis force
Nu	=	local Nusselt number, hD_h/k
Nu_0	=	Nusselt number in fully developed turbulent nonrotating tube flow
Pr	=	Prandtl number
Pr_t	=	turbulent Prandtl number
R	=	radius from axis of rotation
Re	=	Reynolds number, $\rho W_0 D_h/\mu$
Ro	=	rotation number, $\Omega D_h/W_0$
r	=	inner radius of bend
S	=	distance in streamwise direction
T	=	local coolant temperature
T_b	=	coolant bulk temperature
T_0	=	coolant temperature at inlet
T_w	=	wall temperature
W_0	=	inlet velocity
$\Delta\rho/\rho$	=	density ratio, $(T_w - T_0)/T_w$
θ	=	dimensionless temperature, $(T - T_0)/(T_w - T_0)$
μ	=	dynamic viscosity of coolant
ρ	=	density of air
Ω	=	rotational speed in rpm
ω	=	rotational speed, rad/s

Subscripts

b	=	bulk
ce	=	centrifugal
co	=	Coriolis
h	=	hydraulic
t	=	turbulent
w	=	wall
0	=	inlet

Presented as Paper 2004-1276 at the AIAA 42nd Aerospace Sciences Meeting, Reno, NV, 5–8 January 2004; received 29 November 2004; revision received 27 February 2005; accepted for publication 28 February 2005.

*Ph.D., Research Scholar/Scientist and Instructor, Department of Mechanical, Materials and Aerospace Engineering, 4000 Central Florida Boulevard. Member AIAA.

†J. S. Kapat Professor of Mechanical Engineering, and Lockeed Martin Professor of Engineering, Department of Mechanical, Materials and Aerospace Engineering, 4000 Central Florida Boulevard. Associate Fellow AIAA.

Introduction

SUSTAINABLE and cheap sources of energy and water are two of the most important issues for the society of tomorrow. In this aspect turbines and generators, the workhorses that provide energy to millions of houses and factories, will continue to remain important tomorrow. High-speed rotating machines such as heavy-duty gas turbines must be designed for high reliability as any failure in these machines can lead to catastrophic failure in the systems that they support. This is particularly true for generators and turbines in an aircraft. Reliability of any generator and turbine is critically dependent on the temperature rise in their individual components while in operation. For example, it has been observed that the creep life of turbine blades is reduced to half with every 10 to 15°C rise in metal temperature. In other words, hot components design of these machines must aim to keep their operating temperatures within some tolerable limits. To achieve this goal, the hot components are cooled with a combination of advanced cooling techniques. However, one common technique is to have a coolant fluid flowing through internal cooling channels formed within the hot components.

For decades researchers have investigated various aspects of internal cooling in both generators and turbines in order to understand flow and heat-transfer characteristics in these cooling channels so that more optimal and efficient designs can be achieved. One of the particularly difficult aspects of better understanding the associated physical processes has been to understand how turbulence production, dissipation, and transport are affected by rotation inside rotating internal cooling channels used in turbine blades and generator rotors. The basic philosophy of cooling techniques employed

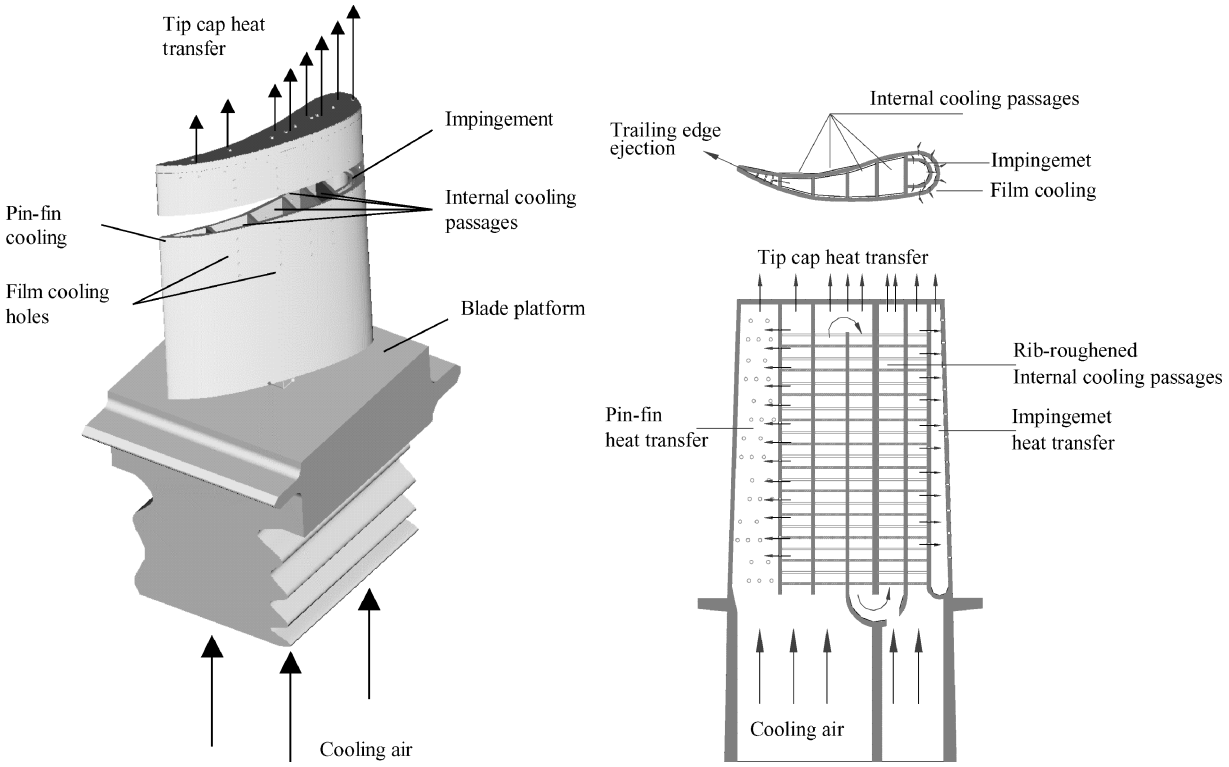

Fig. 1 Three-dimensional view of turbine blade and platform showing a) cooling systems and b) internal cooling turbine-blade configuration.

in the turbine blades and generator rotors is similar, but different in terms of the relative direction of coolant flow with respect to the respective axis of rotation. In gas turbine blades the internal cooling channels are primarily orthogonal to the axis of rotation (orthogonal-mode rotation), wheras in generator rotors the cooling channels are parallel to the axis of rotation (parallel-mode rotation). Moreover, generator rotors and turbine blades use oil and air as coolants, respectively, which have very different properties that can potentially affect turbulence production, dissipation, and transport. In this paper only internal cooling channels in orthogonal-mode rotation are addressed.

The cooling technique currently used for blades of high-pressure turbines is a combination of internal and film cooling. In this technique, cooler air is injected into serpentine passages within the blade. Most of this air issues out of tiny (film-cooling) holes into the high-temperature boundary layer on the blade surface, in an effort to form a cooler layer between the hot gas stream and the blade surface (see Fig. 1).

The blades, in addition to the temperature loads, are however stressed by the rotational forces (i.e., the Coriolis and the centrifugal forces). These rotational induced forces complicate the flow structure within the channel. Figure 2 shows a schematic view of a U-bend section, located in the center of turbine blade. The forces acting on the flowfield and the boundary conditions are shown. The effects of channel walls, corners, bends, ribs, heating, and rotation characterize the flow phenomena inside internal cooling channels of turbine blades.

To enhance the heat-transfer rate, rib tabulators are usually introduced inside internal cooling channel. The use of ribs causes rapid increase in the supply pressure, which is already limited in a turbine and requires high cost for manufacturing. Hence careful optimization is needed to justify the use of ribs. Increasing rotation number Ro is another approach to increase heat-transfer rate to values that are comparable to those achieved by introduction of ribs. One objective of this research is to study the latter approach in order to give insight on the optimum range of application and a possible replacement of the high cost and complex ribs by increasing rotation number.

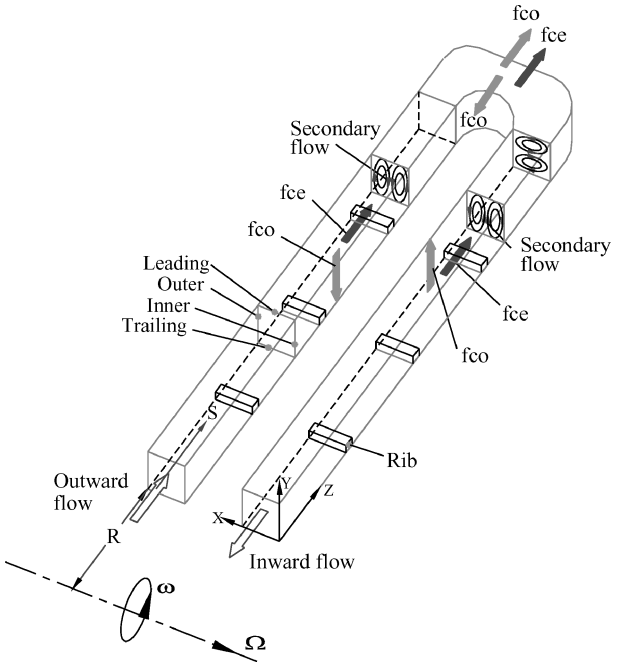

Fig. 2 Schematic view of a U-bend internal cooling channel in the interior of turbine blade.

When performing experiments, in addition to the high cost, it is very difficult to achieve conditions that enable measured data to be dependent on few parameters. In many experiments the level of uncertainty of measurements alters the data. In numerical simulations it is possible to ensure accurate values for all variables and boundary conditions. It is thus important to perform both measurements and numerical simulations to study the flowfield and heat transfer in such complex situations. The most accurate and powerful approach when performing numerical simulation is the direct numerical simulation

(DNS), but not feasible for practical engineering problems because of the large computational cost, and only some fundamental flows can be studied with this approach. Large-eddy simulation (LES) is situated somewhere between DNS and the Reynolds-averaged Navier–Stokes (RANS) approach. Basically large eddies are resolved directly in LES, whereas small eddies are modeled, which results in mesh resolution requirements that are much less restrictive than with DNS; however, extremely fine meshes are still required. Using the RANS approach, the computational cost can be reduced while relatively accurate results can still be produced. Thus in this paper the RANS approach is employed to perform the simulations.

Many research groups have performed studies on channels with smooth walls both experimentally and numerically. This effort, although it has been performed mostly for relatively low rotation numbers and density ratios, is to be addressed in the next section for completeness. In the following section experimental and numerical work of heated rotating channels with smooth walls in orthogonal mode rotation is considered. Special consideration is given to the effect of rotation number and density ratio.

Effect of Rotation Number in Smooth Wall Channels—Experimental Work

Rotation number, by definition, is a relative measure of Coriolis force to the bulk flow inertial force. A higher rotation number signifies Coriolis and buoyancy effects on flow and heat transfer. Wagner et al.[1] found that increasing the rotation number up to 0.475 and density ratio up to 0.13 causes the Nusselt number in the first pass of the trailing side to increase by a factor of four compared to stationary case; however, the heat transfer decreases rapidly in the second pass to the same values as for stationary case. In the leading side the increase by a factor of 1.5 was observed on the second pass and a decrease of heat transfer in the first pass. In the U turn, the heat transfer increased by a factor of more than 4.7 and 4.4 in the trailing and leading sides, respectively. The decrease in the Nusselt number on the second pass of the trailing side and the first pass of the leading side is caused by the decrease in the axial flow and the stabilization of the near-wall flow on the leading side.

(Moore, 1967; Hart, 1971; Wagner and Velkoff, 1972; Johnson et al., 1972; Rothe and Johnson, 1979) cited in Wagner et al.[2] and Bonhoff et al.[3] Many researchers, studied the effect of rotation (with relatively low rotation numbers, less than 0.24) in an unheated circular and rectangular passages and reported secondary flows and stability aspects of the flow.

Effect of Rotation Number in Smooth Wall Channels—Numerical Simulations

All numerical investigations found in open literature were performed for relatively low rotation numbers and density ratios. The main objectives of these investigations were to compare and verify the capabilities of different turbulence models and to study the heat transfer and flow for the same range of rotation numbers and density ratios studied previously experimentally. Majumdar et al.[4] used the $k-\varepsilon$ model to compare predictions with measurements, where the heat-transfer perditions were not so successful. Tekriwal[5] used the extended $k-\varepsilon$ model and showed that the predictions depend on grid distribution and $y+$. Prakash and Zerkle[6] employed the high-Reynolds-number $k-\varepsilon$ model with wall functions approach. They concluded that the $k-\varepsilon$ model heat-transfer predictions were inaccurate and a more refined model is needed. Sathyamurthy et al.[7] used the $k-\varepsilon$ model with wall function treatment to predict flow and heat transfer in a square rotating duct with U turn. They concluded that a more advanced model [Reynolds-stress model (RSM)] with low Reynolds number is needed to predict such a complex flow. Performing computations on a three-pass channel with two U turns, McGrath and Tse[8] concluded that the two-layer $k-\varepsilon$ model showed improvement over the wall functions treatment. Applying a modified $k-\varepsilon$ model, Dutta et al.[9] showed satisfactory predictions on the radial outward flow. Stephens et al.[10] used a $k-\omega$ model to simulate the smooth square duct with U turn. The $k-\omega$ model showed good heat-transfer results agreement with those measured by Wagner et al.,[1] except at the leading surface of the first pass where an overestimation was predicted. Studying duct flow with curvature and rotation, Iacovides and Li[11] used a high-Reynolds-number $k-\varepsilon$ model, high-Reynolds-number algebraic-second-moment (ASM) closure, low-Reynolds-number ASM with the dissipation rate obtained algebraically and low-Reynolds-number RSM with ε transport equation solved over the entire domain. They concluded that the complex flow downstream of the bend is not reproduced well by the low-Reynolds-number RSM for the rotating case. Bohnoff et al.[12] implemented the RSM model using FLUENT commercial code with standard wall functions. The average heat-transfer predictions were close to Wagner et al.[1] except a slight overestimation in the second pass. Chen et al.[13] simulated the case studied previously by Wagner et al.[1] They used a near-wall second-moment closure model and compared it to a two-layer $k-\varepsilon$ model, which performed worse. The comparison with experimental data clearly demonstrated that the secondary flows in rotating two-pass channels have been strongly influenced by the Reynolds-stress anisotropy resulting from the Coriolis and centrifugal buoyancy forces as well as the U-turn wall curvature.

Effect of Density Ratio in Smooth Wall Channels—Experimental Work

Wagner et al.[1] found that increasing the density ratio from 0.07 to 0.22, that is, rotational buoyancy, with Reynolds number of 2.5×10^4, rotation number of 0.24, and rotating radius of 49 hydraulic diameter, causes a 50% increase in heat-transfer ratio in the first-pass trailing surface and a 100% increase in the first-pass leading surface. In the second pass the heat-transfer coefficient increases by increasing density ratio. In the U turn the heat transfer increased by more than 30% on the trailing and leading surfaces.

Many researchers have studied the effect of density ratio without rotation (see Ref. 2 for more references in vertical stationary smooth ducts). Their results were used later in studying flow and heat transfer in rotating machinery.

Combined Effects of Rotation Number and Density Ratio—Experimental Work

Wagner et al.[1] showed that there are no effects of increasing density ratio on Nusselt-number ratio for stationary case because the gravitational buoyancy is negligible and the rotational buoyancy is zero at zero rotation number. Increasing the rotation number to 0.3 and density ratio to 0.22 causes the Nusselt number to increase on the trailing surface of the first pass compared to lower density ratios. In the leading surface of the first pass, heat transfer decreases by increasing rotation number and then increases again, especially with higher density ratios. Wagner et al.[14] attributed the heat-transfer behavior on the leading surface to the combination of buoyancy forces and the stabilization of the near-wall flow and to the Coriolis-driven secondary flow cells at larger rotation numbers. Heat-transfer ratio in the second pass is relatively unaffected by increasing density ratio and rotation number. The thermal boundary layers at the exit of the U turn, that is, near the inlet of the second pass, are thin. The turn-dominated secondary flows and the rotational effects on heat transfer become more prominent with increasing the axial distance from the U turn.

Heat transfer in smooth walls rotating channels has been studied by Mori et al. (1971), Johnson (1978), Lokai and Gunchenko (1979), Morris and Ayhan (1979), Morris (1981) Isakov and Trushin (1983), and Clifford (1985) all (cited in Han et al.[15]). Their investigations have been conducted for low rotation numbers, less than 0.2, and low-density ratio, less than 0.2. However, their results were inconsistent. The test conditions, measurement techniques, and models might be the reason for the inconsistency.

Combined Effects of Rotation Number and Density Ratio—Numerical Simulations:

The predictions by Ekkad et al.,[16] Prakash and Zerkle,[6] and Dutta et al.[9] showed that the increase in heat-transfer coefficient on

the leading surface is related to buoyancy-driven flow separation. Dutta et al.,[17] using the proper inlet conditions of the experiment, obtained satisfactory heat-transfer results using the $k-\varepsilon$ model. Bonhoff et al.[18] and Iacovides et al.[19] studied the same rotating smooth U-bend case using higher-order turbulence models (RSM and ASM, respectively). Similar to previous studies by the University of Manchester Institute of Science and Technology (UMIST) group,[19] the latter employed one-equation model in the near-wall region, while Ref. 18 used standard logarithmic wall function in a commercial code. For a lower-Reynolds-number case, $Re = 2.5 \times 10^4$, Stephens et al.[10] were able to use a large Reynolds number (LRN) $k-\omega$ turbulence model on a 1.1×10^6 mesh for their compressible simulation. The result was in good agreement with the measured data. Bredberg[20] estimated that the required number of nodes on a well-resolved mesh for $k-\omega$ amounted to 2×10^6. Through a number of simplifications, many researchers have been able to reduce the amount of nodes to 1.9×10^6 (Ref. 21).

Literature review clearly reveals that all publicly available studies have been performed for relatively low rotation numbers and density ratios. Correlations for heat-transfer rate from these studies were derived based on low rotation numbers and density ratios, which might be not valid for cases with high rotation numbers and density ratios. Moreover, compared to two-equation turbulence models, RSM accounts for flow anisotropy and rotational-induced body forces and hence provides more accurate results. Thus in this study, RSM is employed for flowfield simulation as it shows acceptable agreement with experimental data with reasonable computational cost. A Fluent computational-fluid-dynamics (CFD) code is used for this simulation. One objective of this research is to study the effect of high rotation number in order to give insight on the optimum range of application and a possible replacement of the high-cost and complex ribs by increasing rotation number. The effect of high-density ratio on heat transfer will be studied and compared to cases with low-density ratios. High rotation numbers, up to 1.29, and high-density ratios, up to 0.4, are considered. Particular attention will be given to how Reynolds stress, turbulence intensity, and pressure drop are affected by Coriolis, buoyancy, and centrifugal forces caused by high rotation and density ratios.

Numerical Approach and RSM with Rotation Effects

In this study a Fluent CFD code is employed to perform the simulation. The numerical solution method used to solve the Navier–Stokes equations is the finite volume method. A control-volume-based technique is used to convert the governing equations to algebraic equations that can be solved numerically. This control-volume technique consists of integrating the governing equations about each control volume, yielding discrete equations that conserve each quantity on a control-volume basis. For complete details of the numerical approach, see the *Fluent User's Guide*, Vol. 6.2.24.

Reynolds-stress model[22,23] is based on RANS equations with the velocities and other solution variables representing ensemble-averaged (or time-averaged) values. For variable-density flows considered here, RANS equations can be interpreted as Favre-averaged Navier–Stokes equations, with the velocities representing mass-averaged values. RSM solves Reynolds stresses, $\tau_{ij} = \overline{u_i' u_j'}$, using individual transport equations. The exact transport equations for the transport of the Reynolds stresses can be written as follows:

$$\frac{\mathrm{D}\tau_{ij}}{\mathrm{D}t} = D_{T,ij} + D_{L,ij} + P_{ij} + G_{ij} + \phi_{ij} - \varepsilon_{ij} + F_{ij} + S \qquad (1)$$

where the left-hand side is given as

$$\frac{\mathrm{D}\tau_{ij}}{\mathrm{D}t} = \frac{\partial}{\partial t}(\rho \overline{u_i' u_j'}) + C_{ij}$$

where $\partial/\partial t(\rho \overline{u_i' u_j'})$ is the local time derivative, C_{ij} the convection term, $D_{T,ij}$ the turbulent diffusion term, $D_{L,ij}$ the molecular (viscous) diffusion term, P_{ij} the stress production term, G_{ij} the buoyancy production term, ϕ_{ij} the pressure-strain term, ε_{ij} the dissipation term, F_{ij} the production term by system rotation, and S the source term. These terms are given as

$$C_{ij} = \frac{\partial}{\partial x_k}(\rho u_k \overline{u_i' u_j'})$$

$$D_{T,ij} = -\frac{\partial}{\partial x_k}[\rho \overline{u_i' u_j' u_k'} + \overline{p(\delta_{kj} u_i' + \delta_{ik} u_j')}]$$

$$D_{L,ij} = \frac{\partial}{\partial x_k}\left[\mu \frac{\partial}{\partial x_k}(\overline{u_i' u_j'})\right]$$

$$P_{ij} = -\rho\left(\overline{u_i' u_k'}\frac{\partial u_j}{\partial x_k} + \overline{u_j' u_k'}\frac{\partial u_i}{\partial x_k}\right)$$

$$G_{ij} = -\rho\beta\left(g_i \overline{u_j'\theta} + g_i \overline{u_i'\theta}\right)$$

$$\phi_{ij} = \overline{p\left(\frac{\partial u_i'}{\partial x_x} + \frac{\partial u_j'}{\partial x_i}\right)}$$

$$F_{ij} = -2\rho\Omega_k\left(\overline{u_j' u_m'}\varepsilon_{ikm} + \overline{u_i' u_m'}\varepsilon_{jkm}\right)$$

$$\varepsilon_{ij} = \frac{2}{3}\delta_{ij}(\rho\varepsilon + Y_M) \qquad (2)$$

where Y_M is an additional dilatation dissipation term according to the model by Sarkar.[24] Note that C_{ij}, $D_{L,ij}$, P_{ij}, and F_{ij} terms do not require any modeling. However, turbulent diffusion $D_{T,Ij}$, buoyancy production G_{ij}, pressure strain ϕ_{ij}, and dissipation ε_{ij} need to be modeled to close the equations. The code provides a variety of options with regard to the turbulence modeling of theses terms. The pressure strain term ϕ_{ij} is modeled according to the proposals by Gibson and Launder, Fu et al., and Launder (see Ref. 24) which decompose the pressure strain term into slow, rapid, and wall reflection terms. The turbulent diffusive transport term $D_{T,i,j}$ is modeled by the generalized gradient-diffusion model of Daly and Harlow.[24] The production terms as a result of buoyancy are modeled as

$$G_{ij} = \beta\frac{\mu_t}{\mathrm{Pr}_t}\left(g_i\frac{\partial T}{\partial x_j} + g_j\frac{\partial T}{\partial x_i}\right) \qquad (3)$$

where Pr_t is the turbulent Prandtl number for energy, μ_t is the turbulent viscosity and β is the coefficient of thermal expansion. The Fluent manual[24] provides more details on modeling other terms.

Results and Discussion

The results for a four-pass square channel with smooth walls tested by Wagner et al.[1] were used in this study for comparison using two of the four passages with one U turn. The geometry of the two-pass channel is shown in Fig. 3. The four walls of the square duct are denoted as the leading, trailing, inner, and outer sides. All walls are heated to a constant temperature. The coolant temperature is T_0 [i.e., $\theta = (T - T_0)/(T_w - T_0) = 0$] at the duct entrance, and the wall temperature was kept constant at $T = T_w(\theta = 1)$ for all sidewalls. Unlike the experiments, a uniform velocity profile was used at the entrance of the channel with a turbulence level of 3%. This assumption influences the development of the boundary layer at the inlet section of the first leg. Thus the highest uncertainty in the calculated heat-transfer data because of this assumption is expected near the inlet. A zero normal pressure gradient is set at the exit of the channel. The density of the fluid is approximated by $\rho = \rho_0 T_0/T$ to account for density variations, whereas viscosity, thermal conductivity, and specific heat properties variations were calculated as functions of temperature. Comparison between the calculations and measurements was made for rotation number of 0.0 and 0.24 and for coolant-to-wall density ratio $\Delta\rho/\rho$ of 0.13 with Reynolds number fixed to 2.5×10^4 based on $Dh = 0.0127$ m. Nusselt numbers were calculated based on the average bulk temperature and normalized with a smooth tube correlation (Kays and Crawford[25]) for fully

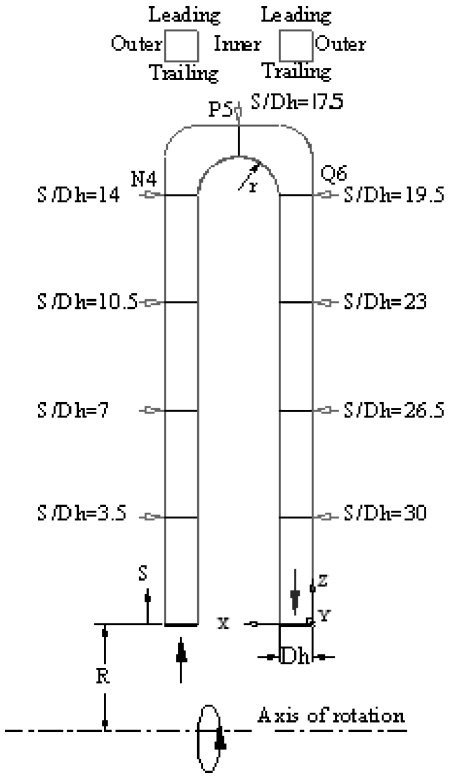

Fig. 3 Geometry for two-pass square channel with smooth walls, $R/Dh = 49$, $r = Dh$.

developed, nonrotating, turbulent flow:

$$Nu_0 = 0.0176Re^{0.8} \tag{4}$$

In the following discussion for all figures, note that $Y/Dh = 0$ corresponds to trailing surface, $Y/Dh = 1$ corresponds to leading surface, $X/Dh = 0$ corresponds to outer surface at location Q6, $X/Dh = 1$ corresponds to inner surface at location Q6, $X/Dh = 3.5$ corresponds to inner surface at location N4, $X/Dh = 4.5$ corresponds to outer surface at location N4, $Z/Dh = 0$ corresponds to inner surface at location P5, and $Z/Dh = 1$ corresponds to outer surface at location P5.

In this study standard wall functions are used for the near-wall treatment of the flow and heat transfer. Enhanced wall treatment is also employed for comparison purposes only. For the pressure interpolation at the faces, the PRESTO scheme was chosen, which showed better results for cases where the pressure profile has a high gradient at the cell face. The minimum convergence criterion for continuity and momentum quantities error was 10E-4 and 10E-7 for the energy equation. A grid-refinement study was performed when standard wall functions were used using four different distributions of $18 \times 18 \times 250$, $25 \times 25 \times 250$, $25 \times 25 \times 390$, and $35 \times 35 \times 250$. The grid refinement in the axial direction showed less than 1% enhancement to normalized Nusselt number. A comparison between calculated and measured values of Nusselt number on the leading- and trailing-edge surface (for $Re = 2.5 \times 10^4$, $R_0 = 0.24$, $\Delta\rho/\rho = 0.13$) showed a maximum of 0.5% changes in Nusselt number between $25 \times 25 \times 250$ and $35 \times 35 \times 250$ grid distribution except for the U turn, where the Nusselt number changed by 1.5%. For RSM with wall functions, the recommended y^+ for the first cell next to a wall is from approximately 12 to 300. Thus the grid of $25 \times 25 \times 250$ was used in this case. With enhanced wall treatment y^+ ranges approximately from 2 to 4. A grid-refinement study in this case was performed using three different grid distributions of $40 \times 40 \times 320$, $40 \times 40 \times 420$, and $52 \times 52 \times 320$ grid points. Figure 4 shows the numerical grid generated using GAMBIT grid generator. Comparison between the calculations and measurements was performed for rotation number of 0.24 and for coolant-to-wall

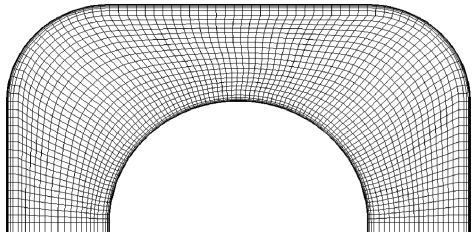

Fig. 4 Numerical grid for channel with smooth walls studied experimentally by Wagner et al.[2]

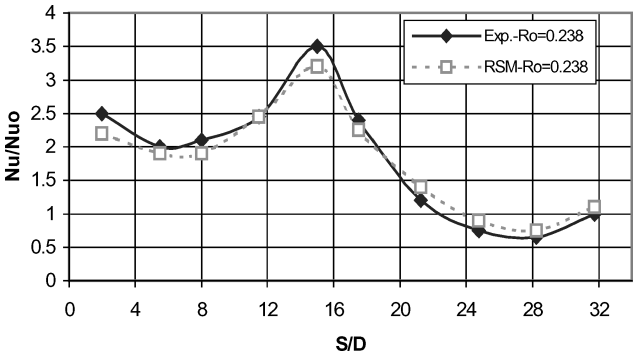

Fig. 5 Predicted and experimental[1] Nusselt-number ratios.

density ratio $\Delta\rho/\rho$ of 0.13. The grid refinement in the axial direction showed less than 1% enhancement to normalized Nusselt number. A comparison between calculated and measured values of Nusselt number on the leading and trailing edge surface (for $Re = 2.5 \times 10^4$, $R_0 = 0.24$, $\Delta\rho/\rho = 0.13$) showed a maximum enhancement of 1% in Nusselt number between $40 \times 40 \times 320$ and $40 \times 40 \times 420$ grid distribution. Increasing the number of grid points on the cross-stream direction showed a maximum of 0.9% changes in Nusselt number between $52 \times 52 \times 320$ and $40 \times 40 \times 320$ grid distribution. Thus all results presented here are based on $40 \times 40 \times 320$ grid points. The difference between predicted and measured Nusselt-number ratios shown in Fig. 5 is about 4%, which is within the experimental uncertainty, except at the channel inlet, where the difference is about 8% because of the difference between the experimental and assumed boundary conditions.

In this study, the range of rotation numbers considered was 0.0, 0.215, 0.43, 0.86, and 1.29. Density ratios of 0.13, 0.229, and 0.4, which correspond to wall temperature of 344, 389, and 500 K, respectively, were studied with a Reynolds number of 2.5×10^4.

Figure 6 shows the results of the Nusselt-number ratio on the leading side of the U channel using five turbulence models compared to experimental data from Wagner et al.[1] All turbulence models predicted the general trend of the Nusselt-number ratio correctly. All models except RSM overestimated the Nusselt-number ratio in the first pass of the U channel and underestimated it in the U turn and second pass. RSM showed enhanced predictions compared to all other four models; thus, all results in the following sections will be presented using the RSM. For a complete detailed comparison between turbulence models, the reader is referred to Ref. 26 where the author showed the advantages of RSM over all other two-equation models. Although validation of RSM was carried out for low rotation numbers of 0.24, with high rotation numbers cases the quality of results will not be affected. This is because of the fundamental advantage of RSM that has exact formulation of the production terms including the rotational induced turbulence terms.

Effect of Rotation Number on Nusselt Number

The effect of rotation on Nusselt-number ratio is shown in Fig. 7 on the leading and Fig. 8 on the trailing side for density ratio of 0.13. In Ref. 2 the results for rotation numbers of up to 0.475 showed that Nusselt number in the trailing surface of the first pass increased by more than a factor of 3.5 and 1.5 in the leading surface of the second

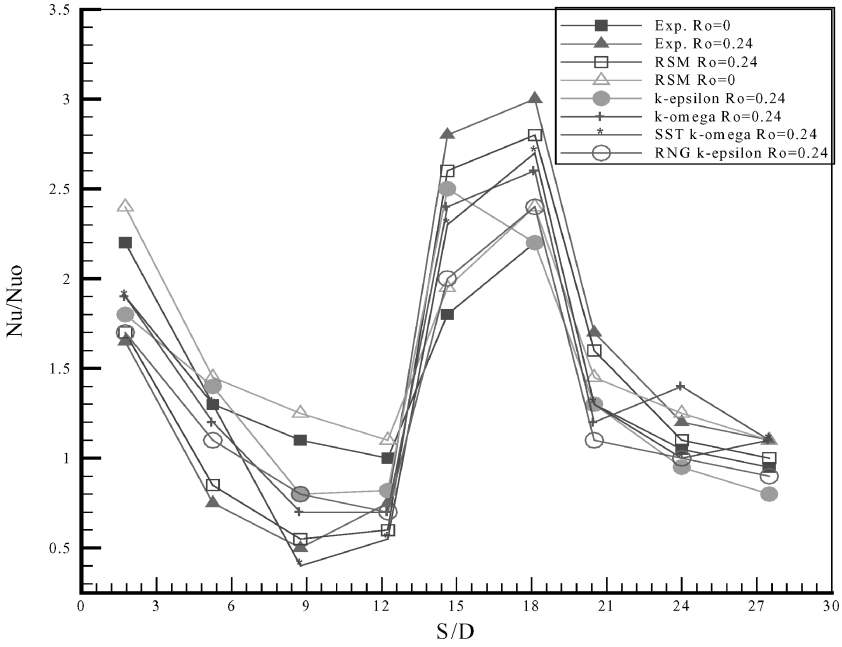

Fig. 6 Nusselt-number ratio on the leading side with $\Delta\rho/\rho = 0.13$.

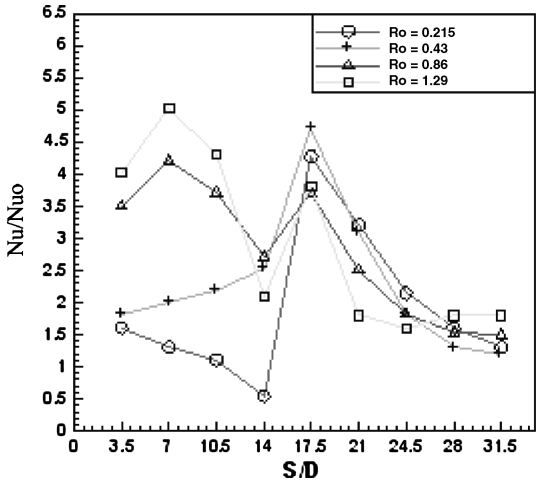

Fig. 7 Leading side $\Delta\rho/\rho = 0.13$.

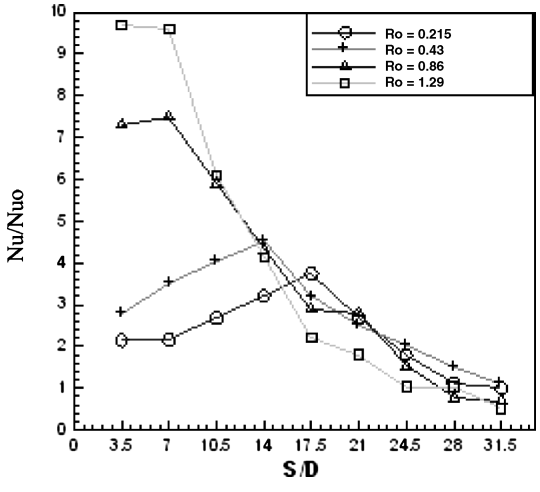

Fig. 8 Trailing side, $\Delta\rho/\rho = 0.13$.

pass. For higher rotation numbers studied here, in the leading side of the first pass the Nusselt-number ratio increases up to 4.2 and 5.3 for rotation numbers of 0.86 and 1.29 respectively and then decreases before and in the U turn and continues to decrease for S/D up to 24.5 then increases slightly near the exit. In the trailing side of the first pass, high rotation has an increasing effect on Nusselt-number ratio by a factor of more than 9 for S/D of up to 7 and decreasing effect after that all of the way to the channel exit. It is clearly shown that under the conditions of high rotation numbers the heat-transfer behavior is different from the case with low rotation numbers. To understand this behavior, the flowfield and heat transfer at a vertical middle line of three planes—in the first pass, in the middle of the U turn, and in the second pass—will be studied further. The effect of high-density ratios will be addressed as well.

Effect of Combined High Rotation and Density Ratio on Nusselt Number

Almost the same values of Nusselt number were predicted for all density ratio cases at high rotation numbers. The Nusselt number increases by a factor of 5.4 at S/D equal 10.5 in the leading side of the first pass (Fig. 9). In the trailing side, the Nusselt number increased up to 7.7 times, whereas for high-density ratio the increase is slightly less. In the leading side of the U turn at S/D of 17.5 (Fig. 10) the increase of the Nusselt number of up to 4.6 times on leading side and 2.8 on trailing side is less than the increase in the first pass.

Finally in the second pass at S/D of 24.5 (Fig. 11), the increase of Nusselt number of up to 2.4 times on leading side and 1.6 on trailing side is much less than on the first pass and the U turn. These results show that at high (compared to low) rotation number and density ratio, the Nusselt number decreased slightly in both leading and trailing sides of the first pass, decreased slightly in leading side, increased on the trailing side of the U turn, increased in the leading side, and decreased in the trailing side of the second pass. It is clearly shown that at high rotation numbers and density ratios the Nusselt number is not increasing, whereas the results in Ref. 1 showed that the Nusselt number is always increasing for the ranges of rotation numbers and density ratios studied. The enhancement in Nusselt number as a result of increasing rotation number is notable and in average is more than the enhancement caused by introduction of ribs when comparing results presented in this study with those available in open literature. To understand this behavior of Nusselt number at high rotation and density ratios, the temperature distribution, velocity profile, secondary flow, turbulence quantities, and

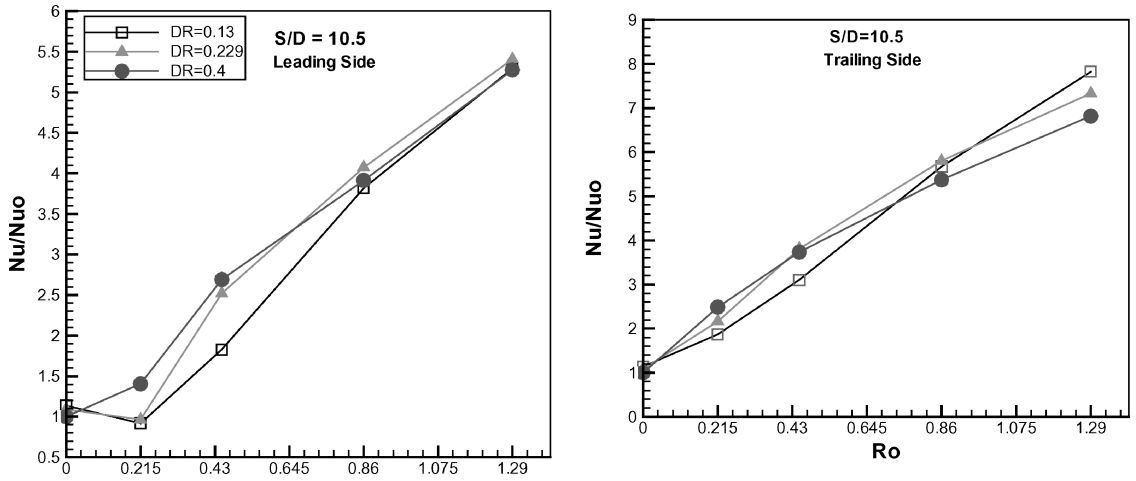

Fig. 9 Nusselt-number ratio in the first pass.

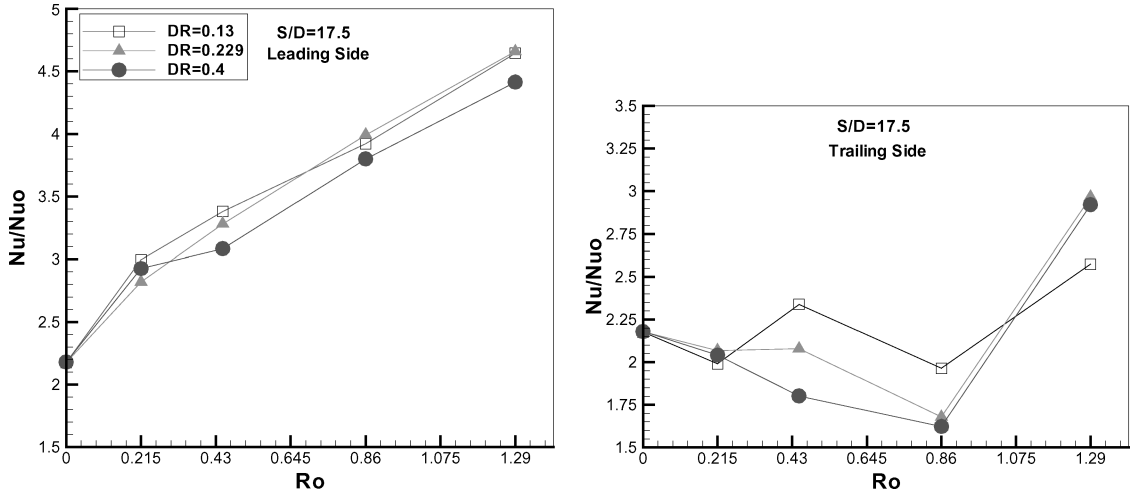

Fig. 10 Nusselt number in the U turn.

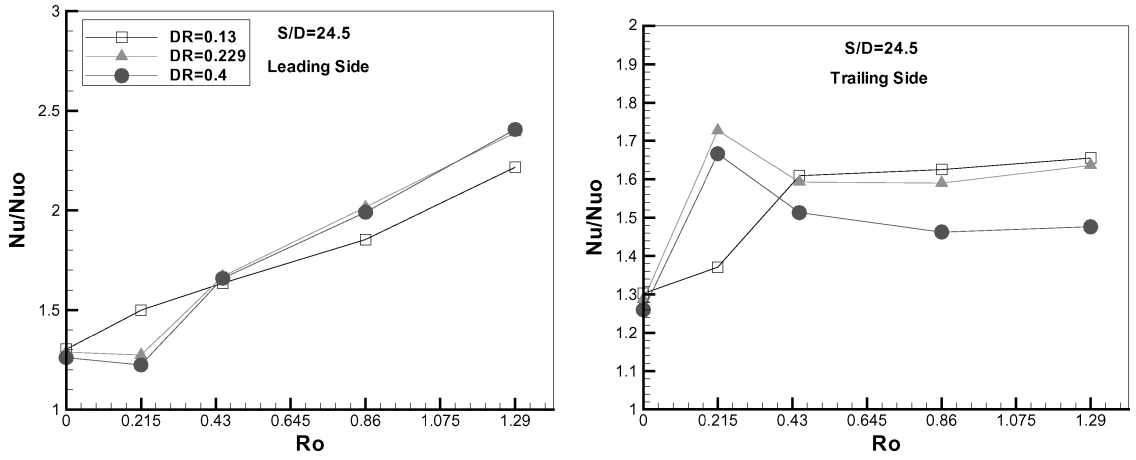

Fig. 11 Nusselt number in the second pass.

pressure drop across the serpentine channel are studied in the next sections.

Discussion of Temperature Distribution and Velocity Profile

The temperature distribution is illustrated in Fig. 12, while the velocity profile is given in Fig. 13. Note that $Y/Dh = 0$ corresponds to trailing side and $Y/Dh = 1$ corresponds to leading side. Note that doubled symbols are used in the legend for all profile data, which explains the stair-step appearance in figures. In the first pass at S/D of 10.5, the fluid velocity near the trailing surface increases by a factor of up to 4.6 times compared to the inlet velocity, whereas strong separation of the flow near the leading surface is predicted by increasing rotation number and density ratio. The minus sign indicates that the flow separates. In the center of the channel ($Y/Dh = 0.5$), the velocity is still in the same order of the inlet velocity for all cases. Increasing the rotation number the Coriolis force that pushes

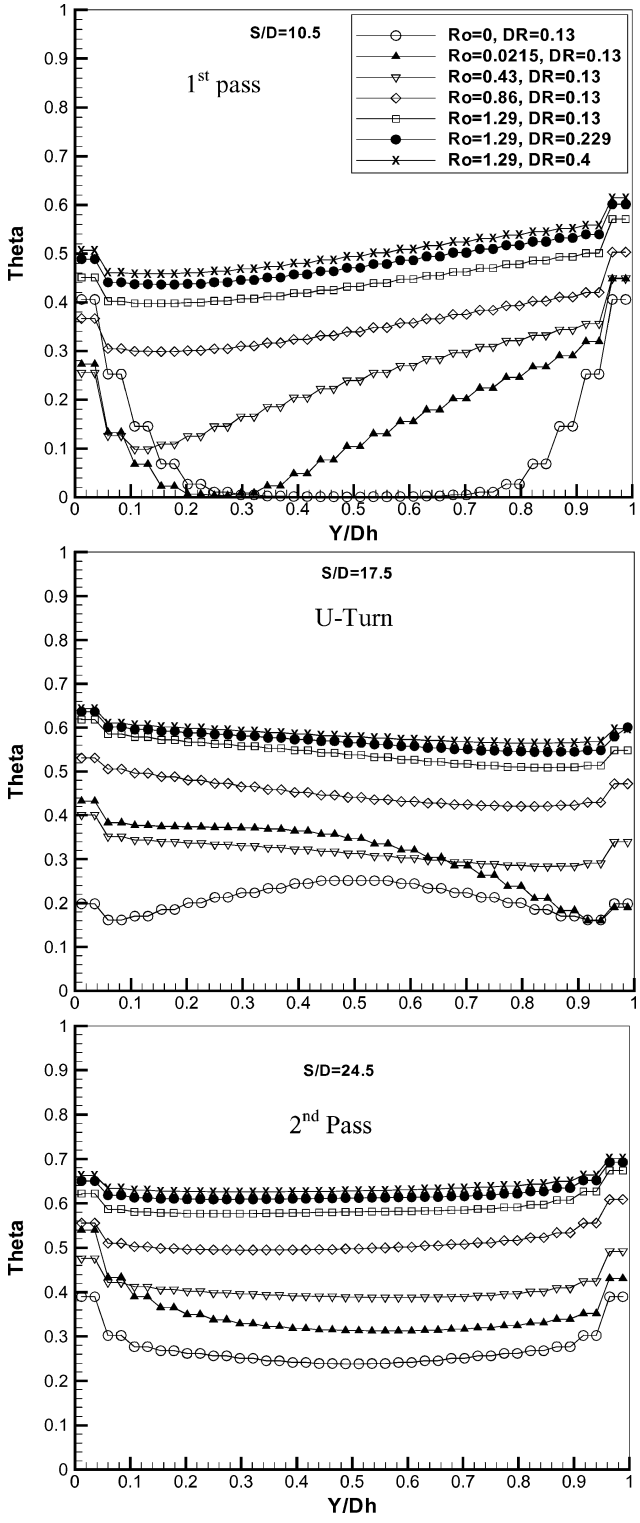

Fig. 12 Temperature distribution.

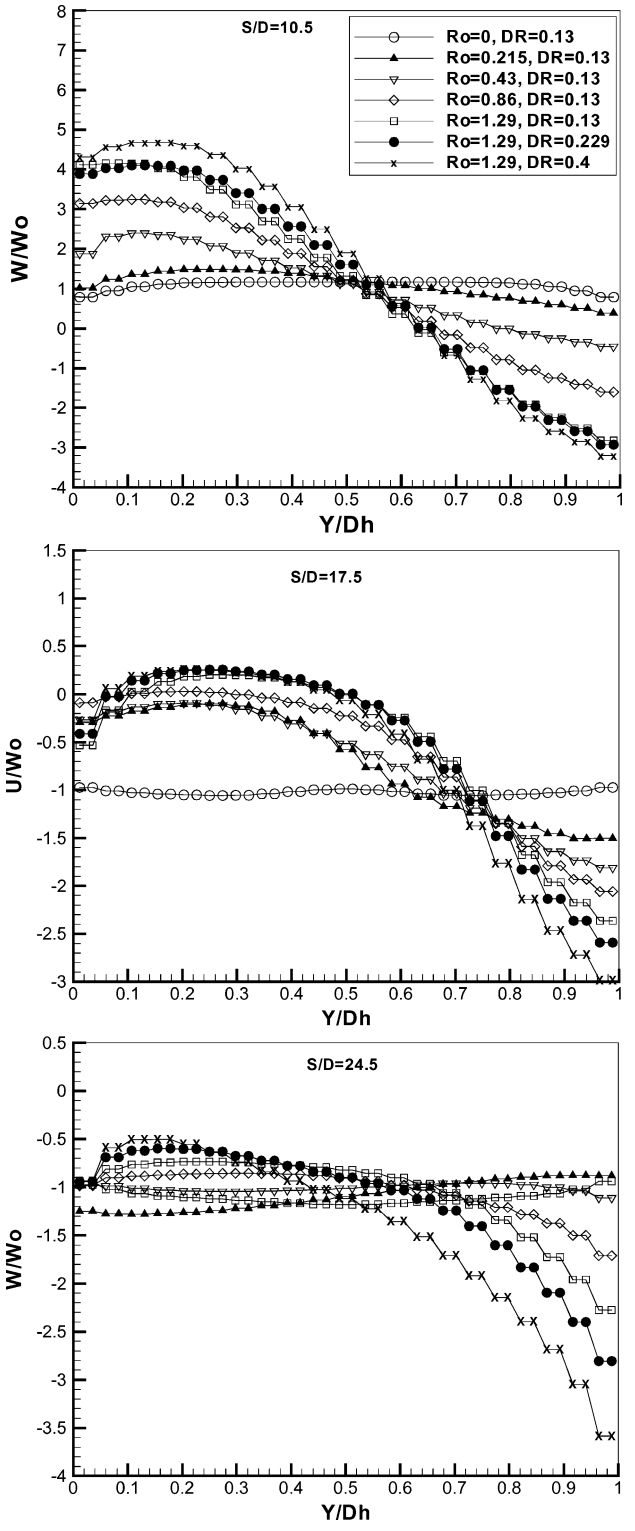

Fig. 13 Streamwise velocity profiles.

the colder fluid towards the trailing surface increases; the increasing centripetal force acting on the direction of the mean flow (outward) tends to push the heavier colder fluid a way from the center of rotation and slow down the hotter fluid near the leading surface. At high rotation numbers this combined effect of the Coriolis and centrifugal forces causes the separation near the leading surface and the acceleration of the flow near the trailing surface, which led to the rapid increase in Nusselt number discussed in the preceding section. In the second pass at S/D of 24.5, the streamwise velocity of the well-mixed fluid increases rapidly at high rotation and buoyancy numbers near the leading side and decreases to low values near the trailing surface. Here the Coriolis force is acting and pushing the fluid with nearly uniform temperature toward the leading surface, whereas the centripetal force acting on the same direction as in the first leg but opposite to mean flow direction tends to slow down the slightly colder and heavier fluid near trailing side and accelerate the lighter fluid near the leading surface. This combined effect of Coriolis and buoyancy forces causes the increase in Nusselt number near the leading side and the decrease near trailing side. The opposite was observed at low rotation numbers, where the fluid near the trailing side is hotter and faster. In the U turn at S/D of 17.5, the hotter fluid near the trailing surface separates at low rotation numbers,

whereas the slightly colder fluid accelerates near the leading surface as rotation and buoyancy numbers increase, which explains the increase in Nusselt number near the leading side.

Secondary Flow

Figure 14 shows the secondary flow for different rotation numbers and density ratios at the center (location P5) and exit (location Q6) of the U turn. At the center of the U turn, Prandtl's secondary flow of the first kind (generated by inviscid effects) caused by rotational Coriolis force is rapidly reduced because the streamwise velocity component U is now parallel to the angular velocity Ω. But the Coriolis force still can be produced by cross-stream component W, which results in small vortex near the trailing outer surface.

As the fluid enters the U turn, the colder, heavier fluid near the trailing surface is accelerated first then the lighter hotter fluid next. This causes Prandtl's secondary flow of the second type (stress-induced), because of the anisotropy of the turbulent Reynolds stresses, to appear in the leading outer corner for $Ro = 0.43$. Increasing rotation number, the corner vortices are suppressed, and the cross-stream secondary motion is govern by the Coriolis force and pressure gradient where a third small vortex appeared near the trailing outer surfaces at $Ro = 1.29$. Increasing density ratio (DR) did not affect the structure of the vortices much. At the U-turn exit (plane Q6) three effects are interacting: the Coriolis force that pushes the cold fluid toward the leading surface, the effect of the circulation in the center of the U bend, and the buoyancy force aligned with meanstream flow. The combined effect of curvature, Coriolis, and centrifugal buoyancy forces resulted in appearance of three vortices (at $Ro = 0.43$): large vortex near the leading, a vortex near the trailing, and a small vortex near the leading outer sides. Increasing rotation number up to 1.29, the Coriolis-induced large vortex dominates, which is shifted downward, and the two small vortices are suppressed. Increasing DR to 0.229, a small vortex appears at the trailing inner corner, and a second vortex appears at the leading inner surface as DR increased to 0.4 as a result of increasing buoyancy.

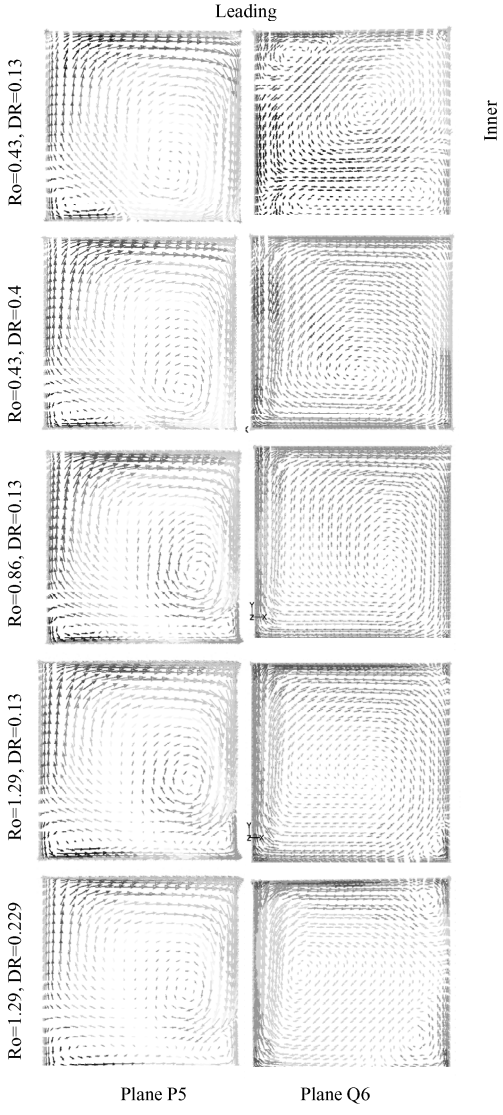

Fig. 14 Secondary flow vectors.

Predicted Reynolds Shear-Stress Components

The shear stresses $\overline{v'w'}$ are depicted in Fig. 15. The reader is referred to Appendix A for discussion on the effect of rotational-induced body forces on Reynolds stresses. At the entrance of the U turn (location N4), high rotation (strong Coriolis) and buoyancy numbers cause the increase of shear stresses near both trailing side (where $V'W' < 0$) and leading side (where $V'W' > 0$), where an increase by a factor of four of that for low rotation numbers was observed at the entrance of the U turn. At the center of the U turn (location P5), increasing rotation number and DR causes a sharp increase in shear stress near the trailing and convex (inner) surfaces (where $V'W' > 0$), decreases them near outer (concave) surface, and increases them near leading surface. At the U-turn exit (location Q6) the turbulence has been greatly damped over a large region, and the higher shear stress is found near the trailing concave (outer) surfaces and with change in sign near the leading surfaces and is mainly caused by increasing both DR and rotation number. As a general trend, it has been observed that the $+veV'W'$ are increasing at high rotation number by increasing DR, whereas for low-rotation-number cases they are decreasing.

The increase in turbulence activity is usually expected to cause an increase in heat-transfer rate. The increase in shear stresses caused by increasing DR just mentioned is not necessarily leading to increase in heat-transfer rate as the fluid temperature, the wall temperature, and the wall heat flux are also important factors that should be considered when observing the heat-transfer behavior.

Normal Reynolds-Stress Components

An important measure of any turbulent flow is how intense the turbulent fluctuations are. This can be quantified in terms of the specific Reynolds-stress components $\overline{u'^2}$, $\overline{v'^2}$, and $\overline{w'^2}$. These three normal stresses can also be regarded as the kinetic energy per unit mass of fluctuating velocity field in the three coordinate directions. These Reynolds stresses are normalized relative to the flow inlet velocity to give the relative turbulence intensity. The normal stresses $\overline{w'^2}$ and $\overline{v'^2}$ are depicted in Figs. 16 and 17, respectively. It has been observed that at the U-turn entrance normal stresses $\overline{w'^2}$ increase by increasing rotation number to 1.29 and density ratio to 0.4 by a factor of 6 near the trailing surface and by a factor of 3 near leading surface compared to the case with $Ro = 0.43$ and DR = 0.13, respectively. The increase in turbulent intensities has a favorable effect on the heat transfer. At the center of the U turn (P5), the normal stresses $\overline{u'^2}$ are still high but less than at the entrance, and the increase in normal stress favors the concave (outer) and leading surfaces. At the U-turn exit the normal stresses $\overline{w'^2}$ are much less in magnitude (turbulence decay), and higher intensities were found near the outer surface, while they are of the same magnitude near leading and trailing surfaces. Observing Figs. 16 and 17, the well-known anisotropy in the normal stresses was observed in all planes, and it was shown in previous work by the author (see Ref. 27). For comparison purposes, the normal stresses $\overline{w'^2}$ are depicted in Fig. 18 using enhanced wall treatment approach for near-wall treatment. It has been observed that at high rotation and buoyancy numbers predictions using wall functions approach are slightly higher in magnitude, but comparable to predictions using enhanced near-wall treatment approach at the centerline of location S/D = 10.5 of the first pass.

No experimental data are available to compare results, but the later results are believed to be more reasonable. However, more studies are being conducted to help explain this behavior.

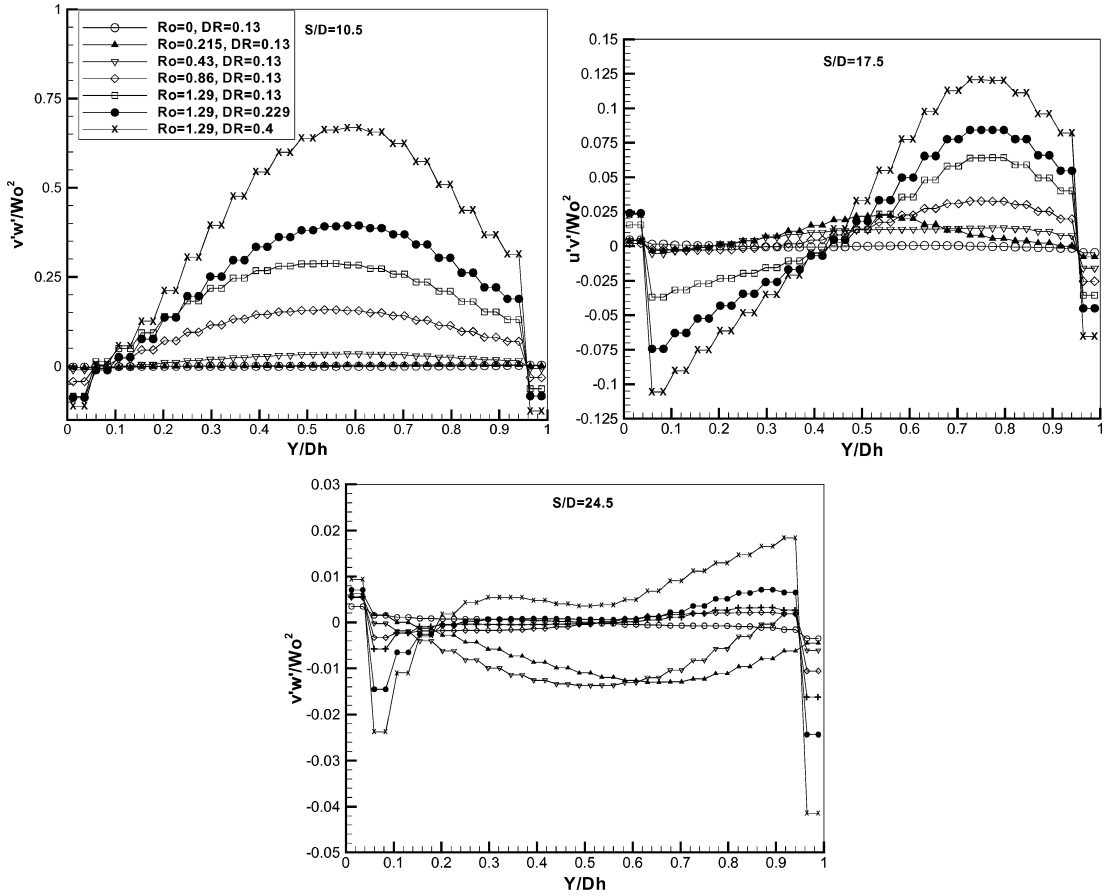

Fig. 15 Reynolds shear-stress components.

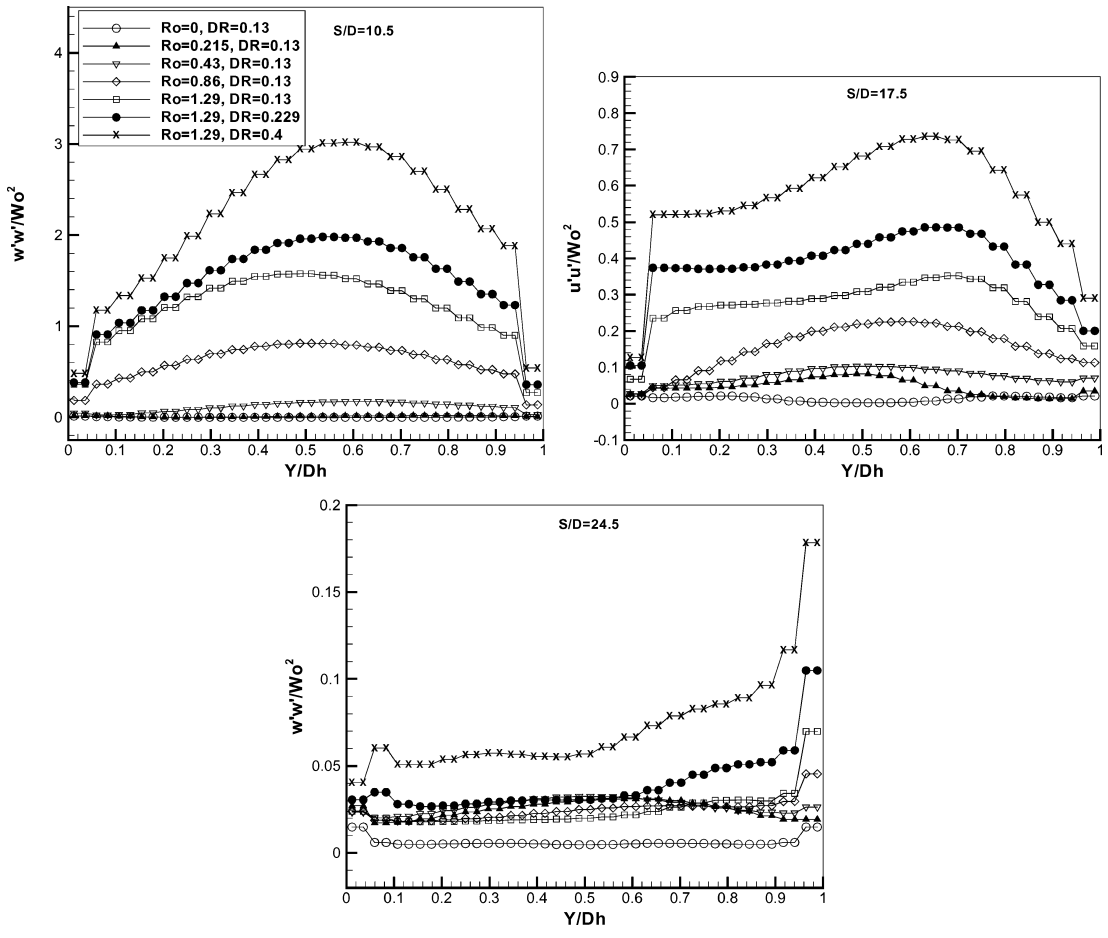

Fig. 16 Streamwise normal stress components using wall functions approach.

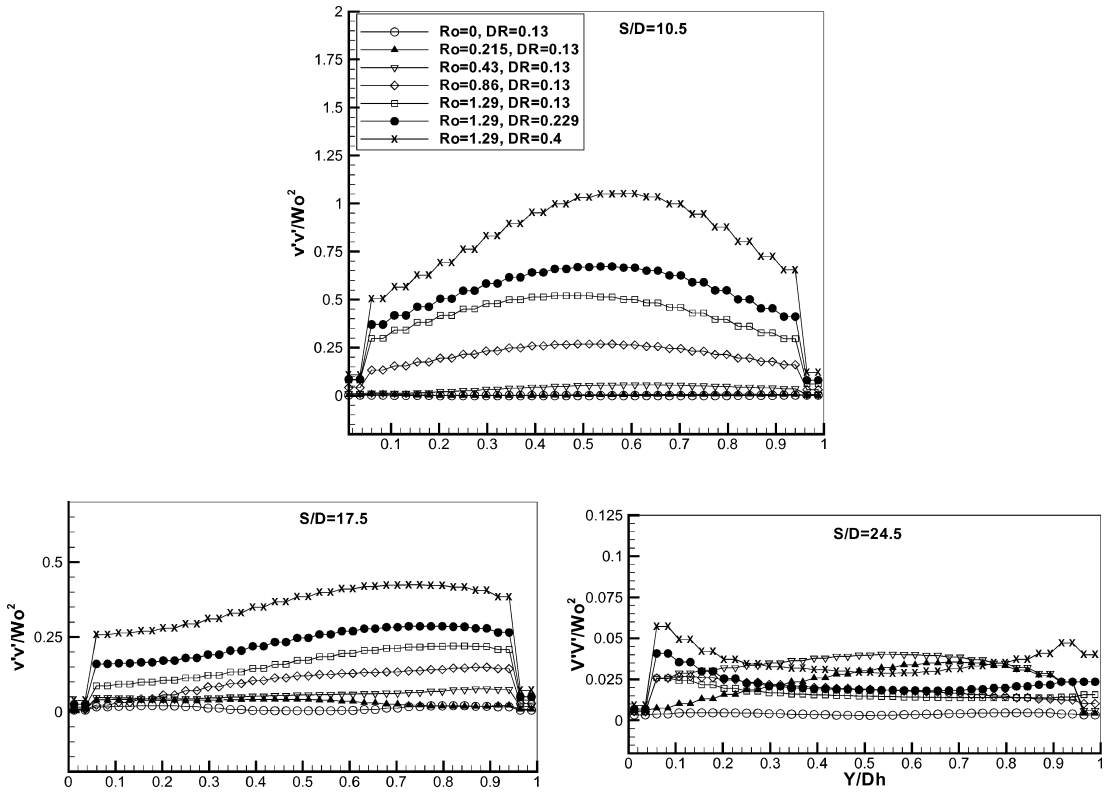

Fig. 17 Vertical normal stress components.

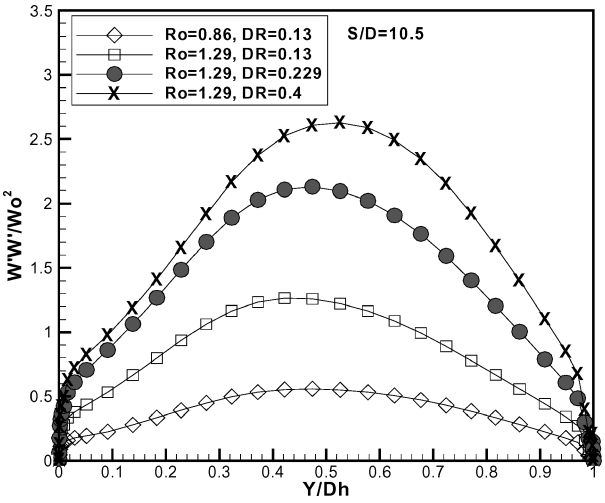

Fig. 18 Streamwise normal stress components using enhanced wall treatment approach.

Total Pressure Drop

The total pressure drop is calculated according to Eq. (5):

$$\left[\left(P_1 + \tfrac{1}{2}\alpha\rho_1 W_1^2\right) - \left(P_S + \tfrac{1}{2}\alpha\rho_S W_S^2\right)\right]$$

$$= \omega^2(\rho_S R_S - \rho_1 R_1) + \text{Losses} \tag{5}$$

where the subscript 1 and S correspond to inlet and location in the streamwise direction, respectively.

Figure 19 shows the mass-weighted average pressure drop across the channel. In the first pass the total pressure increases as the rotation number increases to reach the maximum value in the U turn, then starts to decrease in the second pass. Increasing DR for the same rotation number decreases the total pressure as the density of the fluid is decreasing. When DR increases to 0.23 and 0.4 at the exit of the channel, $R_S = R_1$, but ρ_S is much less than ρ_1, which means that $\omega^2(\rho_S R_S - \rho_1 R_1)$ is less than when DR = 0.13 and hence the pressure gain is more.

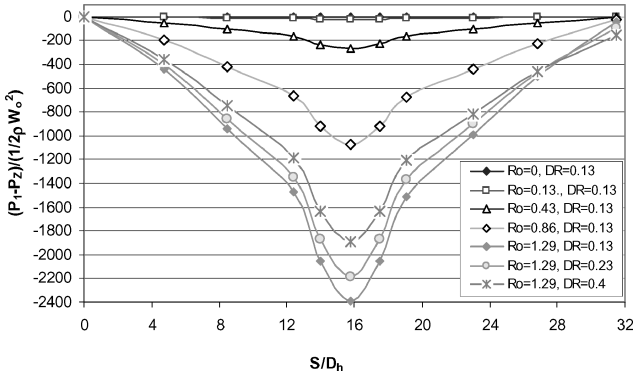

Fig. 19 Total pressure drop—smooth walls channel.

Conclusions

This study examines the rich interplay of physics under the simultaneous actions of Coriolis and centrifugal/buoyancy forces in one of the most challenging internal flow configurations. Several important conclusions are reached from this computational study that can have far-reaching implications on how turbine blades are currently designed.

Two-equation turbulence models overestimated the Nusselt-number ratio in the first pass of the U channel and underestimated it in the U turn and second pass of the cooling channel. The RSM showed better agreement with experimental data than the two-equation models. As opposed to wall functions approach, predictions using the enhanced wall treatment approach are more accurate.

In the first pass of the internal cooling channel, the combined effect of the Coriolis and centrifugal forces causes the separation near the leading surface and the acceleration of the flow near the trailing surface, which led to the rapid increase in Nusselt number. In the second pass the streamwise velocity of the well-mixed fluid increases rapidly at high rotation number and density ratios near the leading side and decreases to low values near the trailing surface. The opposite was observed at low rotation numbers.

Increasing rotation number always increases Nusselt number, whereas increasing DR at high rotation number dose not increase Nusselt number and in some locations even decreases the Nusselt number. The increasing thermal boundary-layer thickness near walls is the possible reason for this behavior of Nusselt number.

Increasing rotation number and DR caused a rapid increase in shear stress and turbulence intensities mainly caused by increasing both rotation number and DR. The well-known anisotropy in the normal stresses was observed in all planes.

The heat-transfer rate can be enhanced rapidly by increasing the rotation number to values that are comparable to the enhancement because of the introduction of ribs inside the internal cooling channels. It is possible to derive a linear correlation for the increase in Nusselt number as a function of rotation number.

Appendix: A

The system rotation at angular velocity Ω^* is manifested in the velocity fluctuation equation by the appearance of a Coriolis force term, $-2(\Omega^* x V)$. The derived equation for the production term by system rotation will take the form

$$F_{ij} = -2\rho\Omega_k\left(\overline{u'_j u'_m}\varepsilon_{ikm} + \overline{u'_i u'_m}\varepsilon_{jkm}\right) \tag{A1}$$

In case of orthogonal-mode rotation, the influence of Eq. (A1) on the dynamics is to be investigated next. With a rotation vector $\Omega^* = (-\Omega i + 0j + 0k)$, it follows from Eq. (A1) that the Reynolds-stress equations contain additional terms as shown in Table A1.

Because, nominally, $\overline{w'w'} > \overline{v'v'}$in channel flow; thus, in the first pass F32 is negative, in which case it acts to add to Reynolds shear stress where $(\overline{w'v'} < 0)$ and decrease it, where $(\overline{w'v'} > 0)$. Enhanced Reynolds shear stress can be associated with high turbulence activity, and hence the trailing side in the first pass is unstable (pressure side), and the leading (suction side) is stable and the opposite on the second leg.

To study why the Coriolis force has that kind of effect on the Reynolds shear stress, consider the part of F32 that depends on $\overline{w'w'}$. This term has arisen from multiplying the Coriolis term—$2(-\Omega_t W)$ by W. The expression $-2(-\Omega_t W)$ represents a force deflecting $W > 0$ motions toward the trailing surface and motions $W < 0$ toward the leading surface. In other words, $W > 0$ motions are accompanied by a move negative V, whereas $W < 0$ motions make V move positive. Thus it is not surprising that the Reynolds shear stress is amplified on the trailing side and decreases on the leading side.

Similarly, the term $2\rho\Omega\overline{v'^2}$ in F32 acts to diminish the Reynolds shear stress. In this case the Coriolis force $-2(-\Omega_t V)$, deflects motion in the $\pm Y$ directions toward the $\pm Z$ directions, respectively, which leads to reduce the Reynolds stress. The cumulative effect of the two processes represented in F32 is to enhance Reynolds stress on the trailing side while decreasing it on the leading side because the V fluctuations are smaller than the W fluctuations, and hence the corresponding Coriolis effect is smaller.

In $\overline{w'w'}$ equation there is an extra production term $4\rho\Omega\overline{w'v'}$ and an equal and opposite term in the $\overline{v'v'}$equation. When $\overline{w'v'}$ is negative, that rotation diminishes $\overline{w'w'}$and enhances $\overline{v'v'}$ on the trailing side and vice versa on the leading side. For high rotation-number value, it can happen that $\overline{w'w'} < \overline{v'v'}$, in which case, according to F32 equation, there is no new effect of rotation on enhancing or diminishing Reynolds stress.

Because F33 in $\overline{w'w'}$ equation appears with equal and opposite magnitude to F22 in the $\overline{v'v'}$ normal Reynolds-stress equation, there is clearly no net effect of rotation in the turbulent kinetic energy equation. Moreover, rotation effects do not appear in the mean momentum equation, except indirectly through the action of the Reynolds shear stress. Consequently, there is no mechanism by which a model such as the $k-\varepsilon$ model is able to account for the effects of rotation in a channel flow. Clearly, the minimum requirement necessary to do so is to have the capacity to model the anisotropy of the Reynolds-stress tensor in unidirectional mean flows. Only more advanced models such as the Reynolds-stress model (RSM) are rotationally useful for treating rotating channel flow. Also a good quality of results depends strongly on the attention paid to the near-wall modeling.

To illustrate the fundamental advantage of the exact formulation of the production terms in RSM compared to eddy-viscosity models, consider Pij and Fij production terms. The k equation $(k = 0.5(\overline{u'u'} + \overline{v'v'} + \overline{w'w'})$ is unaffected by rotation as $\mathrm{F33} + \mathrm{F22} = 0$. In addition, the shear stress $\overline{w'v'}$ is inaccurately estimated by neglecting the rotational production F32 because of the isotropic estimation of the normal stresses $\overline{w'w'} = \overline{v'v'}$. This clearly suggests that EVMs should include ad hoc modifications to correctly predict rotational-induced turbulence.[28,29]

References

[1]Wagner, J. H., Johnson, B. V., and Kopper, F. C.,"Heat Transfer in Rotating Serpentine Passages with Smooth Walls," *Journal of Turbomachinery*, Vol. 113, July 1991, pp. 321–330.

[2]Wagner, J. H., Johnson, B. V., and Hajek, T., "Heat Transfer in Rotating Passages with Smooth Walls and Radial Outward Flow," *Journal of Turbomachinery*, Vol. 113, Jan. 1991, pp. 42–51.

[3]Bonhoff, B., Tomm, U., Johnson, B., and Jennions, I.,"Heat Transfer Predictions for Rotating u-Shaped Coolant Channels with Skewed Ribs and with Smooth Walls," Paper 97-GT-162, American Society of Mechanical Engineers, New York, June 1997.

[4]Majumdar, A. K., Pratap, V. S., and Spalding, D. B.,"Numerical Computation of Flow in Rotating Ducts," *Journal of Fluids Engineering*, Vol. 99, No. 7, 1977, pp. 148–153.

[5]Tekriwal, P., "Heat Transfer Predictions with Extended $k-e$, Turbulence Model in Radial Cooling Ducts Rotating in Orthogonal Mode," *Journal of Heat Transfer*, Vol. 116, May 1994, pp. 369–380.

[6]Prakash, C., and Zerkle, R, "Prediction of Turbulent Flow and Heat Transfer in a Radially Rotating Duct," *Journal of Turbomachinery*, Vol. 114, Jan. 1992, pp. 835–846.

[7]Sathyamurthy, P. S., Karki, K. C., and Patankar, S. V., "Prediction of Turbulent Flow and Heat Transfer in a Rotating Square Duct with a 180 Degree Bend," American Society of Mechanics Engineers, Paper 94-GT-197, July 1994.

[8]McGrath, D. M., and Tse, D. G., "A Combined Experimental/Computational Study of Flow in Turbine Blade Cooling Passage. Part 2. Numerical Simulations," American Society of Mechanics Engineers, Paper 95-GT-149, July 1995.

[9]Dutta, S., Andrews, M. J., and Han, J. C., "Prediction of Turbulent Heat Transfer in Rotating Smooth Square Ducts," *International Journal of Heat and Mass Transfer*, Vol. 39, No. 12, 1996, pp. 2505–2514.

[10]Stephens, M. A., Shih, T. I., and Civinskas, K. C., "Computations of Flow and Heat Transfer in a Rotating U-Shaped Square Duct with Smooth Walls," AIAA Paper 96-3161, July 1996.

[11]Iacovides, H., Launder, B. E., and Li, H.-Y., "The Computation of Flow Development Through Stationary and Rotating U-Duct of Strong Curvature," *International Journal of Heat and Fluid Flow*, Vol. 17, No. 5, 1996, pp. 22–33.

[12]Bonhoff, B., Tomm, U., Johnson, B. V., and Jennions, I.,"Heat Transfer Predictions for Rotating U-Shaped Coolant Channels with Skewed Ribs and

Table A1 Influence of Fij on dynamics in orthogonal-mode rotation

	First Pass			U turn			Second Pass	
i, j	Reynolds stress	Fij	i, j	Reynolds stress	Fij	i, j	Reynolds stress	Fij
3,3	$\overline{w'w'}$	$4\rho\Omega\overline{w'v'}$	1,1	$\overline{u'u'}$	0	3,3	$\overline{w'w'}$	$4\rho\Omega\overline{w'v'}$
2,2	$\overline{v'v'}$	$-4\rho\Omega\overline{v'w'}$	2,2	$\overline{v'v'}$	$-4\rho\Omega\overline{v'w'}$	2,2	$\overline{v'v'}$	$-4\rho\Omega\overline{v'w'}$
3,2	$\overline{w'v'}$	$2\rho\Omega(\overline{v'^2} - \overline{w'^2})$	1,2	$\overline{u'v'}$	$-2\rho\Omega\overline{u'w'}$	3,2	$\overline{w'v'}$	$2\rho\Omega(\overline{v'^2} - \overline{w'^2})$

with Smooth Walls," American Society of Mechanics Engineers, Paper 97-GT-162, July 1997.

[13]Chen, H. C., Jang, Y. J., and Han, J. C.,"Computation of Heat Transfer in Rotating Two-Pass Square Channels by a Second-Moment Closure Model," *International Journal of Heat and Mass Transfer*, Vol. 43, No. 9, 2000, pp. 1603–1616.

[14]Wagner, J. H., Johnson, B. V., Graziani, R. A., and Yeh, F. C., "Heat Transfer in Rotating Serpentine Passages with Trips Normal to the Flow," *Journal of Turbomachinery*, Vol. 114, No. 4, 1992, pp. 847–857.

[15]Han, J. C., Dutta, S., and Srinath, E., *Gas Turbine Heat Transfer and Cooling Technology*, Taylor and Francis, New York, 2000, Chap. 4.

[16]Ekkad, S. V., Huang, Y., and Han, J. C., "Detailed Heat Transfer Distributions in Two-Pass Smooth and Turbulated Square Channels with Bleed Holes," *Fundamentals of Augmented Single-Phase Convection*, Vol. 330, 1996, pp. 133–140.

[17]Dutta, S., Andrews, M. J., and Han, J. C., "Prediction of Turbulent Flow and Heat Transfer in Rotating Square and Rectangular Smooth Channels," *Journal of Thermophysics and Heat Transfer*, Vol. 11, No. 2, 1997, pp. 318, 319.

[18]Bonhoff, B., Schneider, T., Johnson, B., and Jennions, I., "Prediction for Turbulent Flow in Rotating and Non Rotating Coolant Channels," Paper, Oct. 1997.

[19]Iacovides, H., Launder, B. E., and Li, H. Y., "The Computation of Flow Development Through Stationary and Rotating U-Ducts of Strong Curvature," *International Journal of Heat and Fluid Flow*, Vol. 117, No. 4, 1996, pp. 22–33.

[20]Bredberg, J., "Turbulence Modelling for Internal Cooling of Gas. Turbine Blades," Ph.D. Dissertation, Dept. of Thermo and Fluid Dynamics, Chalmers Univ. of Technology, Göteborg; Sweden, Aug. 2002.

[21]Vogal, J. C., and Eaton, J. K., "Combined Heat Transfer and Fluid Dynamic Measurements Downstream of a Backward-Facing Step," *Journal of Heat Transfer*, Vol. 107, Jan. 1985, pp. 922–929.

[22]Gibson, M. M., and Launder, B. E., "Ground Effects on Pressure Fluctuations in the Atmospheric Boundary Layer," *Journal of Fluid Mechanics*, Vol. 86, 1978, pp. 491–511.

[23]Launder, B. E., and Shima, N., "Second-Moment Closure for the near-Wall Sublayer: Development and Application," *AIAA Journal*, Vol. 27, No. 10, 1989, pp. 1319–1325.

[24]*The FLUENT User's Guide*, ver. 6.2, FLEUNT, Lebannon, NH, 2004.

[25]Kays, W. M., and Crawford, M. E., *Convective Heat and Mass Transfer*, 3rd ed, McGraw–Hill, 1993, Chap. 13–14.

[26]Sleiti, A. K., "Effect of Coriolis and Centrifugal Forces on Turbulence and Transport at High Rotation and Buoyancy Numbers," Ph.D. Dissertation, Mechanical, Materials and Aerospace Dept., Univ. of Central Florida, Orlando, May 2004.

[27]Sleiti, A. K., and Kapat, J. S.,"Effect of Coriolis and Centrifugal Forces on Turbulence and Transport at High Rotation and Buoyancy Numbers in Smooth Internal Cooling Channels," AIAA Paper 2004-1276, Jan. 2004.

[28]Wolfstein, M., "The Velocity and Temperature Distribution of One-Dimensional Flow with Turbulence Augmentation and Pressure Gradient," *International Journal of Heat and Mass Transfer*, Vol. 12, No. 1, 1969, p. 318.

[29]Huser, A., Biringen, S., and Hatay, F. F., "Direct Simulation of Turbulent Flow in a Square Duct: Reynolds-Stress Budget," *Physics of Fluids*, Vol. 6, No. 2, 1994, pp. 3144–3152.